Optimized Gen-II FeCrAl cladding production in large quantity for campaign testing

Yukinori Yamamoto
Zhiqian Sun
Bruce A. Pint
Kurt A. Terrani

June 3rd, 2016

OAK RIDGE NATIONAL LABORATORY
MANAGED BY UT-BATTELLE FOR THE US DEPARTMENT OF ENERGY

ORNL/TM-2016/227

Fuel Cycle Research and Development, Advanced LWR Fuels

Optimized Gen-II FeCrAl cladding production in large quantity for campaign testing

Yukinori Yamamoto, Zhiqian Sun, Bruce A. Pint, Kurt A. Terrani

Date Published: June 3rd, 2016

Work Package Title: ATF Cladding Production
Work Package #: FT-16OR02020213
Work Package Manager: Yukinori Yamamoto
Milestone #: M3FT-16OR020202132

Prepared under the direction of the
U.S. Department of Energy
Office of Nuclear Energy
Fuel Cycle Research and Development
Advanced LWR Fuels

Prepared by
OAK RIDGE NATIONAL LABORATORY
Oak Ridge, TN 37831-6283
managed by
UT-BATTELLE, LLC
for the
US DEPARTMENT OF ENERGY
under contract DE-AC05-00OR22725

CONTENTS

LIST OF FIGURES

Figure	Page

LIST OF TABLES

This page intentionally left blank

ACKNOWLEDGMENTS

This page intentionally left blank

ABSTRACT

There are two major objectives in this report; (1) to optimize microstructure control of ATF FeCrAl alloys during tube drawing processes, and (2) to provide an update on the progress of ATF FeCrAl tube production via commercial manufacturers.

Experimental efforts have been made to optimize the process parameters balancing the tube fabricability, especially for tube drawing processes, and microstructure control of the final tube products. Lab-scale sheet materials of Gen II FeCrAl alloys (Mo-containing and Nb-containing FeCrAl alloys) were used in the study, combined with a stepwise warm-rolling process and intermediate annealing, aiming to simulate the tube drawing process in a commercial tube manufacturer. The intermediate annealing at 650ºC for 1h was suggested for the tube-drawing process of Mo-containing FeCrAl alloys because it successfully softened the material by recovering the work hardening introduced through the rolling step, without inducing grain coarsening due to recrystallization. The final tube product is expected to have stabilized deformed microstructure providing the improved tensile properties with sufficient ductility. Optimization efforts on Nb-containing FeCrAl alloys focused on the effect of alloying additions and annealing conditions on the stability of deformed microstructure. Relationships between the second-phase precipitates (Fe_2Nb-Laves phase) and microstructure stability are discussed.

FeCrAl tube production through commercial tube manufacturers is currently in progress. Three different manufacturers, Century Tubes, Inc. (CTI), Rhenium Alloys, Inc. (RAI), and Superior Tube Company, Inc. (STC), are providing capabilities for cold-drawing, warm-drawing, and HPTR cold-pilgering, respectively. The first two companies are currently working on large quantity tube production (expected 250 ft length) of Gen I model FeCrAl alloy (B136Y3, at CTI) and Gen II (C35M4, at RAI), with the process parameters obtained from the experimental efforts. The expected delivery dates are at the end of July, 2016, and the middle of June, 2016, respectively. Tube production at STC would be the first attempt to apply cold-pilgering to the FeCrAl alloys. Communication has been initiated, and the materials have been machined for the cold-pilgering process.

1. INTRODUCTION

The development of nuclear-grade enhanced accident tolerant fuel (ATF) cladding alloys targets a new, metal-base structural material for nuclear fuel cladding in Light Water Reactors (LWR). These materials will replace the current zirconium-based alloy fuel cladding and should exhibit greatly improved accident tolerance, including good mechanical properties across a wide temperature range in addition to excellent oxidation and radiation resistance under normal and transient operating conditions. FeCrAl alloys were selected based on their excellent oxidation resistance in high temperature steam environments up to 1475°C (provided by the sufficient amounts of Cr and Al additions), compared to the industry standard zirconium alloys which do not have such high temperature tolerances [1,2,3,4]. This is the key for enhancing safety margins under severe accident conditions by limiting heat and hydrogen production, which occur when the fuel cladding reacts with steam during a severe accident [5]. With superior high temperature strength compared to zirconium alloys, utilization of this class of alloys is expected to enhance burst margins during design basis accident scenarios and potentially for conditions extending beyond those limits.

Development efforts for ATF FeCrAl alloys were initiated in FY2013 under the Fuel Cycle Research and Development (FCRD) program, which consisted of two distinct phases, each evaluating a different alloy generation; in Phase 1: Gen I model FeCrAl alloys, and in Phase 2: Gen II modified FeCrAl alloys [6]. In Phase 1, the Gen I model FeCrAl alloys, consisting of quaternary Fe-Cr-Al-Y alloys, were used for property screening as a function of Cr and Al content. A base alloy composition of Fe-13Cr-4.5Al-Y was down-selected based on experimental findings demonstrating good balance between mechanical properties, oxidation resistance, irradiation resistance, weldability, and so on [7,8,9,10] . In Phase 2, minor alloying additions were applied with guidance from computational thermodynamics for improved strength together with sufficient oxidation resistance at elevated temperatures, without sacrificing acceptable fabricability to support FeCrAl thin-wall tube product with commercial manufacturers. The comprehensive summary of the Gen II modified FeCrAl alloy development and property evaluation can be found in the reports previously submitted [11,12,13].

In LWRs, a seamless tube product is required for the fuel cladding which typically has a length of ~4 m with an outer diameter of ~10 mm. In the case of FeCrAl alloys, a wall-thickness of less than 0.4 mm is also suggested for reducing potential neutronic impact compared to current zirconium alloy cladding [14]. The FeCrAl cladding should also be structurally sound with sufficient mechanical properties at both service temperature and accident conditions. These requirements impose considerable technical challenges for tube fabrication processes of FeCrAl alloys. Research has been performed to achieve a balance between high-temperature performance and tube fabricability in newly developed FeCrAl alloys. BCC-Fe materials with Cr and Al additions typically suffer from poor ductility because of relatively high ductile-brittle transition temperature [15]. Microstructural stability of the refined grain or subgrain structure at high temperature is critical to maintain both the fabricability of the alloys during tube production processes and the mechanical properties of the final tube products.

There are two different approaches to fabricate a seamless thin-wall tube commercially: tube-drawing and pilgering – both shown in Figure 1 [16,17]. The tube-drawing process is widely applied for making thin-wall tubes used in various industries: architectures, boilers, petrochemical and chemical plants, nuclear and fossil energy plants, aerospace, vehicles, medical equipment, appliances, etc. A die and mandrel are required to reduce and control the outer diameter (OD) and the inner diameter (ID) as shown in Figure 1a. Tube drawing is occasionally conducted under warm conditions (up to ~300°C), depending on the die and mandrel materials, to make the fabrication process easier.

Pilgering was developed for manufacturing tubing with ultrathin walls for nuclear fuel cladding in the 1950's [18]. The high-precision tube roller (HPTR) method provides a fast, economical way to achieve extreme reductions in diameter and wall thickness. The vertical mass ring (VMR) die method uses a couple of rotating dies with varying radius for smooth tube deformation to achieve a more than 90% cross-sectional reduction in a single working cycle. Both pilgering approaches can be categorized as compressive production routes similar to a conventional rolling process, and are suitable for applying larger deformation than tube-drawing processes, although they typically require a large capital investment and are not feasible for the production of small quantities of tubing.
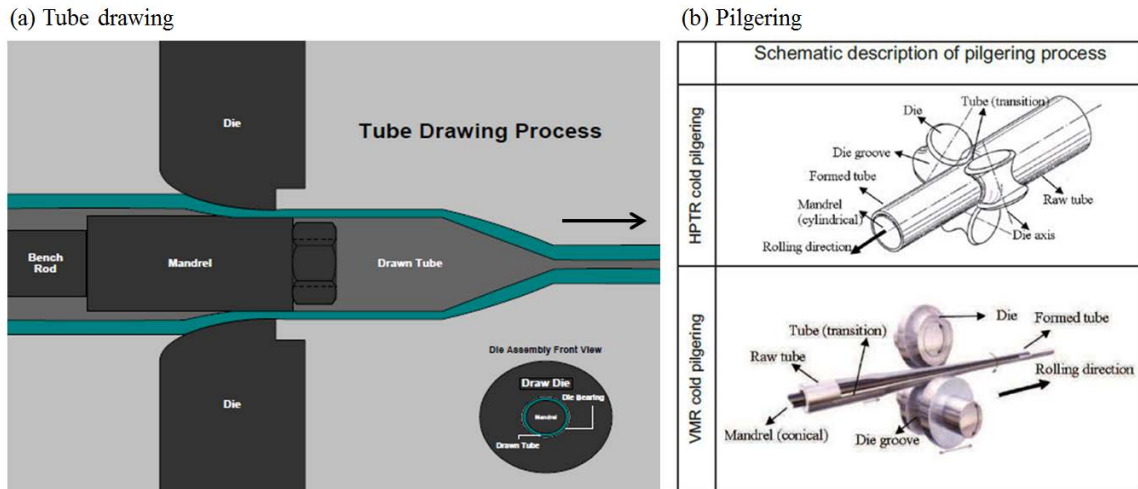
Figure 1. Commercial thin-wall tube fabrication processes; (a) tube drawing with a mandrel [16], and (b) pilgering [17]. Note that HPTR and VMR stand for "high-precision tube roller" and "vertical mass ring die", respectively.

There are two major objectives in this report; (1) to optimize process parameters of the tube drawing process for a large-quantity production of ATF FeCrAl thin-wall tubes by commercial manufacturers, and (2) to report on the progress of ATF FeCrAl tube production via commercial manufacturers. The first part of the report focuses on microstructure evolution and hardness evaluation of selected FeCrAl alloys during simulated tube fabrication processes with various process parameters. In order to optimize fabricability and mechanical properties of the FeCrAl alloys in the final tube products the required processing window had to be defined. The study was conducted using lab-scale sheet materials with warm-rolling processes to simulate the applied deformation and microstructure evolution during the warm-drawing and annealing process to enable direct transfer of these results to large-quantity tube production. The second objective is to report on tube production progress with three commercial tube manufacturers, Century Tubes, Inc. (CTI), Rhenium Alloys, Inc. (RAI), and Superior Tube Company, Inc. (STC), with capabilities of cold-drawing, warm-drawing, and HPTR cold-pilgering, respectively. The first two companies have conducted the FeCrAl alloy tube production since FY2014 under subcontract with the current FCRD projects, and they are currently working on large-quantity tube production (expected 250 ft. length) of Gen I (CTI) and Gen II (RAI). The most-recent progress on tube production is described. Tube production at STC will be challenging since it is the first attempt to apply cold-pilgering to the developed ATF FeCrAl alloys under the current project. The materials provided to STC were identical to those processed at CTI (Gen II FeCrAl alloys) to enable direct comparison between tube-drawing and pilgering. These details are described in this report.

2. EXPERIMENTAL PROCEDURES

2.1 Microstructure Control Study

Two different series of Gen II ATF FeCrAl alloys were used in the microstructure control study; Mo-containing alloys and Nb-containing alloys. The nominal alloy compositions were mostly based on Fe-13Cr-(5.2 or 6)Al-0.2Si-Y, in wt.%, with the additions of 2Mo or (0.7-2)Nb. The effect(s) of varying the Cr content was also examined in the Nb containing alloys. Analyzed compositions of the alloys are summarized in Table 1.

Table 1. Analyzed compositions of alloys studied.

ID	Composition, wt.%										
	Fe	Cr	Al	Y	Mo	Si	Nb	C	S	O	N
C35M3	79.43	13.06	5.31	0.053	2.00	0.13	<0.01	0.001	<0.0003	0.0012	0.0003
C35M4-1	79.63	12.91	5.22	0.060	1.98	0.20	-	<0.01	0.001	-	-
C35M4-2	79.56	12.89	5.25	0.040	2.06	0.20	-	<0.01	0.001	-	-
C36M2	78.40	13.00	6.29	0.059	1.99	0.20	<0.01	0.001	<0.0003	0.001	0.0004
C16N	81.72	11.08	5.95	0.045	<0.01	0.19	0.99	0.005	0.0008	0.0013	0.0003
C26N	80.75	12.10	5.96	0.027	<0.01	0.17	0.98	0.005	0.0009	0.0013	0.0004
C36N	79.74	13.11	5.94	0.058	<0.01	0.15	0.98	0.004	0.001	0.0015	0.0003
C36N2	78.82	13.00	5.94	0.055	<0.01	0.20	1.97	0.004	0.001	0.0021	0.0004
C36N3	80.19	12.75	6.08	0.040	<0.01	0.19	0.66	0.003	0.0008	0.0009	0.0007

The Mo-containing alloy ingots were vacuum induction melted by Sophisticated Alloys, Inc. (SAI), Butler, PA. SAI has vacuum induction melt furnaces with capacities up to 500 lbs. Two heats of Mo-containing alloys, C35M3 and C35M4, were used in this study. There were two different heats of "C35M4" prepared for the large-quantity FeCrAl tube manufacturing study (Table 1). Heat "C35M4-2" was used in the microstructure control study. C36M2 (Fe-13Cr-6Al-2Mo) was prepared as a reference material for the microstructural stability study. All alloys were homogenized at 1200°C for up to 4 h in argon cover gas, followed by rapid cooling (air cooling + water quenching) to room temperature. The ingots were extruded at 800°C at ORNL (C35M3 and C36M2) or 1050°C at SAI (C35M4-1 and -2), followed by straightening and centerless grinding to make bar samples with 23-25 mm diameters. The ground bars were then annealed at 800°C for more than 30 min to create an equiaxed grain structure (80-100 µm). These bar samples were used as starting materials or master bars for both the microstructure control study and tube manufacturing, respectively.

Nb-containing FeCrAl alloys were prepared by arc-melting and drop-casting. The lab-scale heats with 13 mm x 25 mm x 125 mm dimensions were homogenized at 1200°C for up to 2 h in Ar cover gas, followed by hot-forging, rolling, and annealing at the same temperature to prepare 2.5 mm thick plates with an equiaxed grain structure (~100 µm). These plate samples were used as starting materials for both microstructure control studies.

2.2 Tube Production with Commercial Manufacturers

Table 2 shows the processes/products and the commercial manufacturers utilized to conduct the ATF FeCrAl tube-drawing production including alloy casting, master bar/tube production through extrusion,

gun drilling, and tube drawing. Table 3 lists the alloys provided to the manufacturers while Table 4 summarizes the analyzed alloy compositions that were used for the tube production efforts. The cast ingots are provided by SAI. The ingots are homogenized and hot extruded to make bar (or tube) shapes and to control the initial microstructure for the subsequent drawing process. The extrusion process with trial heats was conducted at ORNL (for B126Y, C06M2, and C36M3). SAI also performed the extrusion process (for B136Y3 and C35M4). The extruded bars require a gun-drilling process to make the master tubes to be drawn. This was conducted by Century Tubes, Inc. (San Diego, CA) or Rhenium Alloys, Inc. (North Ridgeville, OH) for trial heat tube fabrication. For large-quantity production, Grover Gundrilling, LLC (Oxford, ME) performed the gun-drilling task. The tube drawing process is being conducted by CTI and RAI working with LANL/ORNL and ORNL, respectively. In a parallel tube-drawing effort, ORNL is currently working with Superior Tube Company, Inc. (Collegeville, PA) to apply HPTR cold-pilgering for alloys C06M2 and C36M3.

Table 2. List of commercial manufacturers for thin-wall FeCrAl tube production

Process/product	Manufacturer	Remarks
Cast ingots (>20 lbs.)	Sophisticated Alloys, Inc. (Butler, PA)	Vacuum induction melt, up to 500 lbs.
Hot extrusion	ORNL	For trial heats, 1250 ton press
	Sophisticated Alloys, Inc. (Butler, PA)	For large quantity production
Gun drilling	Rhenium Alloys, Inc. (North Ridgeville, OH)	For trial heats
	Grover Gundrilling, LCC (Oxford, ME)	For large quantity production
Tube drawing	Century Tubes, Inc. (San Diego, CA)	Cold drawing, work with LANL/ORNL
	Rhenium Alloys, Inc. (North Ridgeville, OH)	Warm drawing, work with ORNL
Pilgering	Superior Tube Company, Inc. (Collegeville, PA)	Cold pilgering, work ORNL

Table 3. Manufacturer list and plan status for tube production

Manufacturer	Alloys	Remarks
Century Tubes	B126Y, B136Y2*, C06M2, C36M3	B126Y and C06M2 were delivered through LANL; B136Y2 and C36M3 are in progress.
Rhenium Alloys	C35M4*	In progress
Superior Tube	C06M2, C36M3	In progress

*aim to produce total 250 ft length

Table 4. Analyzed compositions of the alloys for tube production

ID	Composition, wt.%										
	Fe	**Cr**	**Al**	**Y**	**Mo**	**Si**	**Nb**	C	S	O	N
B126Y	**81.99**	**11.99**	**5.98**	**0.020**	-	-	-	0.003	0.0004	0.0045	0.0003
B136Y3-1	**80.81**	**12.97**	**6.19**	**0.030**	-	-	-	<0.01	0.001	-	-
B136Y3-2	**80.72**	**13.01**	**6.24**	**0.030**	-	-	-	<0.01	0.001	-	-
C06M2	**81.84**	**9.88**	**6.03**	**0.050**	**1.97**	**0.21**	**<0.01**	0.003	<0.01	<0.01	<0.0005
C35M4-1	**79.63**	**12.91**	**5.22**	**0.060**	**1.98**	**0.20**	-	<0.01	0.001	-	-
C35M4-2	**79.56**	**12.89**	**5.25**	**0.040**	**2.06**	**0.20**	-	<0.01	0.001	-	-
C36M3	**78.8**	**12.98**	**6**	**0.040**	**1.98**	**0.18**	**<0.01**	0.003	<0.0003	0.0016	0.0002

3.   OPTIMIZATION OF MICROSTRUCTURE CONTROL DURING TUBE DRAWING

3.1   Effect of Annealing Temperatures on Warm-rolled C35M3

The effects of annealing on microstructures and mechanical properties of deformed C35M3 (Gen II, Fe-13Cr-5.2Al-2Mo base) with 10%, 20% and 40% initial strain were investigated. The results indicated the need for intermediate annealing at 650ºC for 1h after each tube-drawing step in order to (1) eliminate potential premature failure during the drawing process, and (2) prevent unnecessary grain coarsening. A stepwise warm rolling process on a C35M3 sheet specimen at 300ºC with intermediate annealing at 650ºC/1h, simulating the actual tube-drawing process, verified the improved fabricability of C35M3 with annealing.

A hot-rolled and annealed C35M3 plate with an equiaxed grain structure (~80 um grains) was prepared as a starting material for the study. The initial Vickers hardness value was 206 ± 2. Three initial thickness reductions (10%, 20%, and 40%) were made via warm-rolling at 300ºC with 10% thickness reduction per pass. The Vickers hardnesses of as-rolled C35M3 plates were 263 ± 4 (for 10%), 297 ± 10 (for 20%), and 322 ± 5 (for 40%). Figure 2 shows the annealing effects on the Vickers hardness of C35M3 in the temperature range of 550-750ºC. Overall, the hardness decreased with longer annealing time mainly due to a recovery process (i.e. annihilation of dislocations and point defects) of the deformed materials. Lower hardnesses were achieved with higher annealing temperatures at a given annealing time and initial strain. At 550° and 650ºC, the hardness values increased proportional to initial strain at a given annealing time. However, this was not the case at 750ºC. As shown in Figure 2, the C35M3 alloy with 40% initial strain annealed for 1h at 750ºC had the lowest hardness value (203 ± 4).
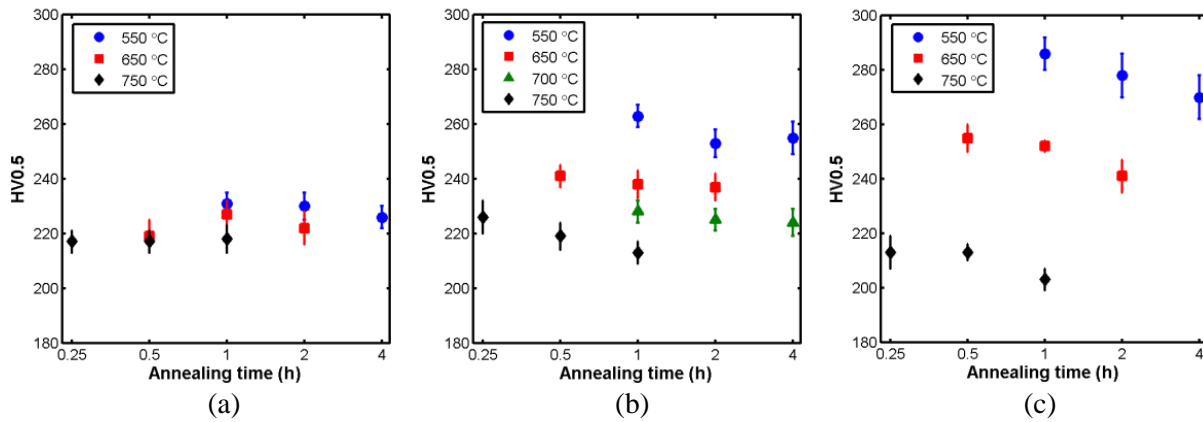
Figure 2. Effects of annealing at 550-750ºC on the Vickers hardness of C35M3 with initial strains of (a) 10%, (b) 20%, and (c) 40%.

Representative optical micrographs of the as-rolled and annealed C35M3 are displayed in Figure 3, Figure 4, and Figure 5. No obvious microstructural changes were observed in C35M3 with 10% initial strain after annealing at the designated conditions (Figure 3). However, with 20% initial strain, a grain spheroidization and non-uniform grain growth was observed after annealing at 750 ºC, as shown in Figure 4. For even larger initial strain (40%), a full recrystallization was observed in C35M3 annealed at 750 ºC (Figure 5). Most likely microstructural changes occurred with annealing temperatures at or higher than 700ºC with the 40% initial strain. Meanwhile, annealing at 650ºC-1h considerably softened C35M3, as shown in Figure 2. These results suggest that the intermediate annealing at 650ºC for 1h would sufficiently soften the materials to allow further deformation (i.e., next tube-drawing step) without grain coarsening via recrystallization during tube fabrications.

(a)　　　　　　　　　　　　　　　　　　(b)

(c)　　　　　　　　　　　　　　　　　　(d)
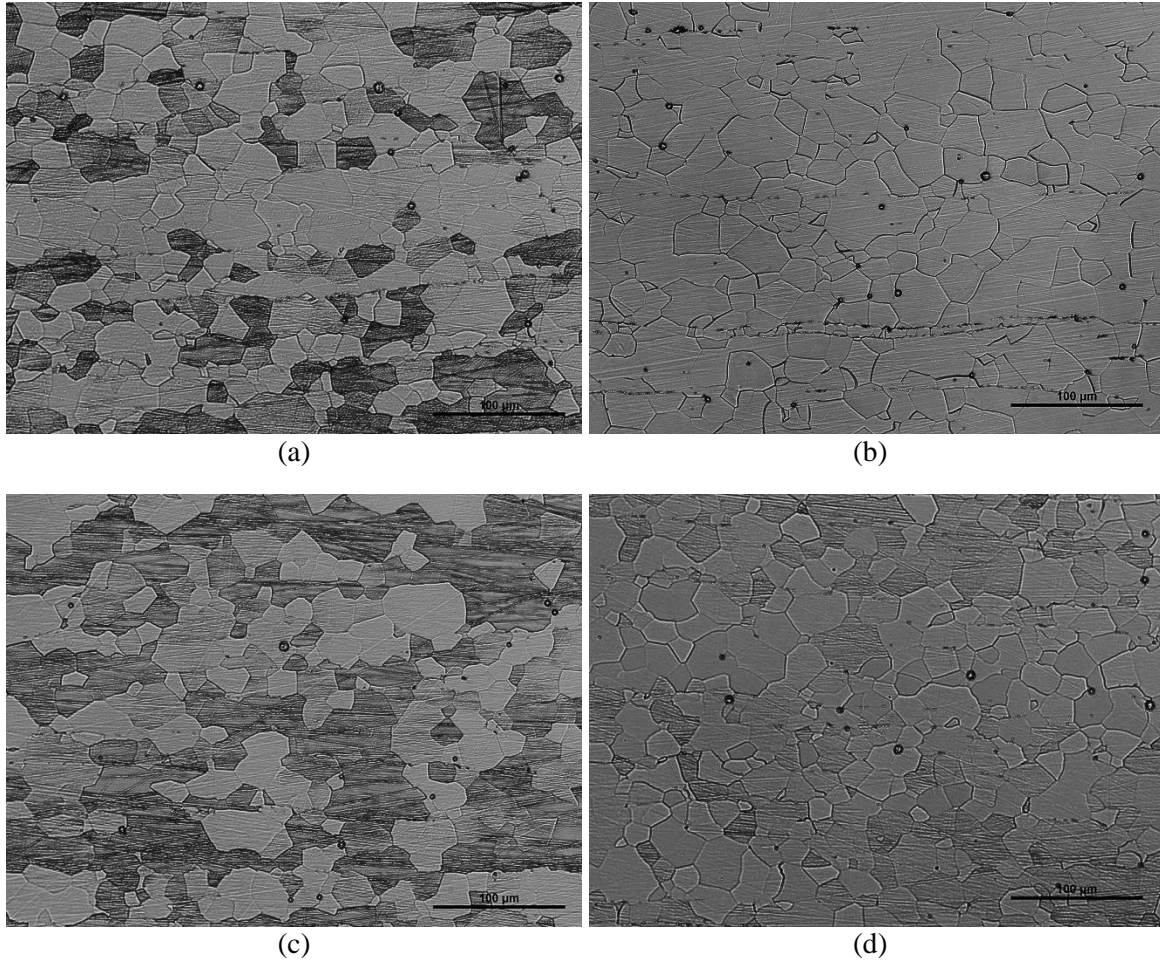
Figure 3. Optical micrographs of the C35M3 samples with the initial thickness reduction of 10%: (a) as-rolled; (b) annealed 4h at 550ºC; (c) annealed 2h at 650ºC; and (d) annealed 1h at 750ºC.
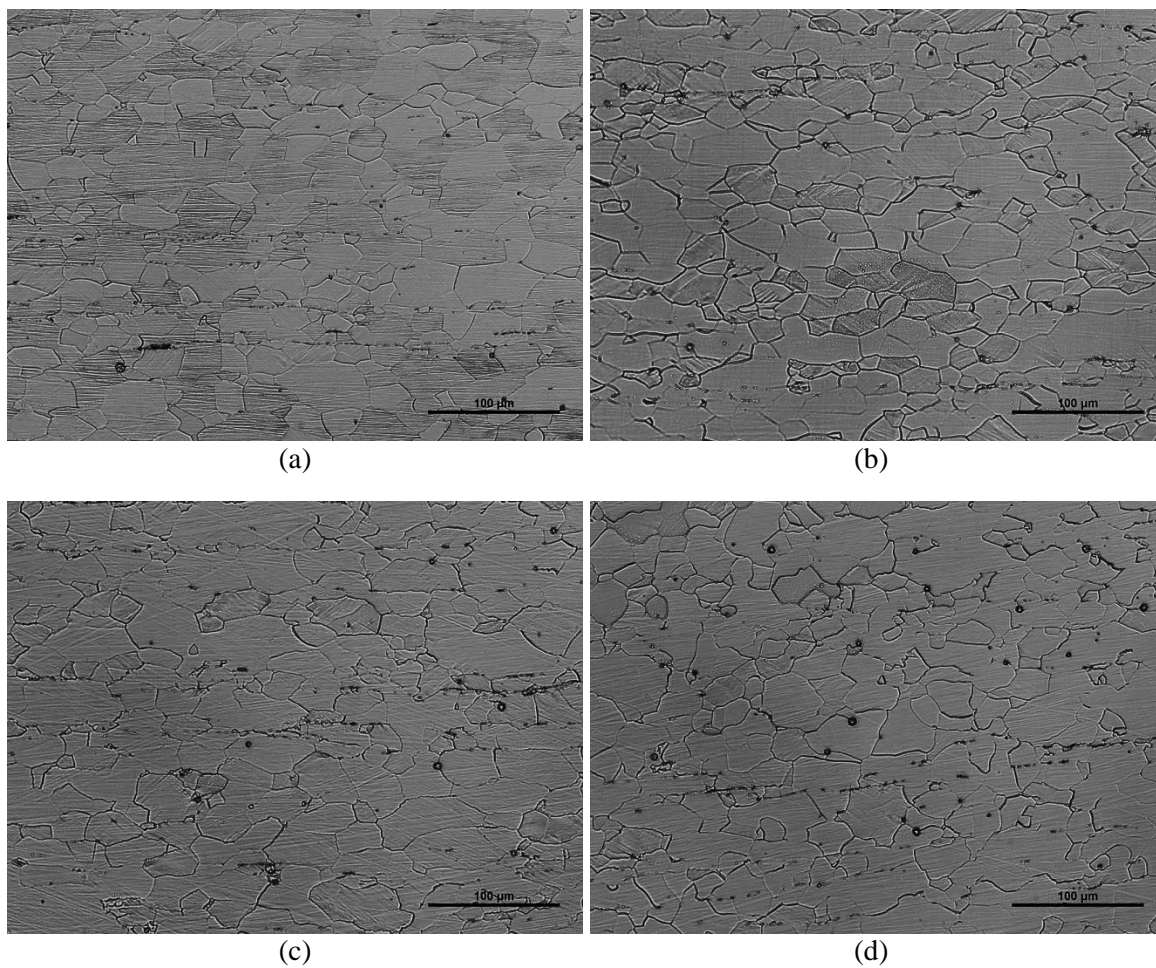
Figure 4. Optical micrographs of the C35M3 samples with the initial thickness reduction of 20%: (a) as-rolled; (b) annealed 4h at 550ºC; (c) annealed 2h at 700ºC; and (d) annealed 1h at 750ºC.

<div align="center">(a)</div>

<div align="center">(b)</div>

<div align="center">(c)</div>

<div align="center">(d)</div>
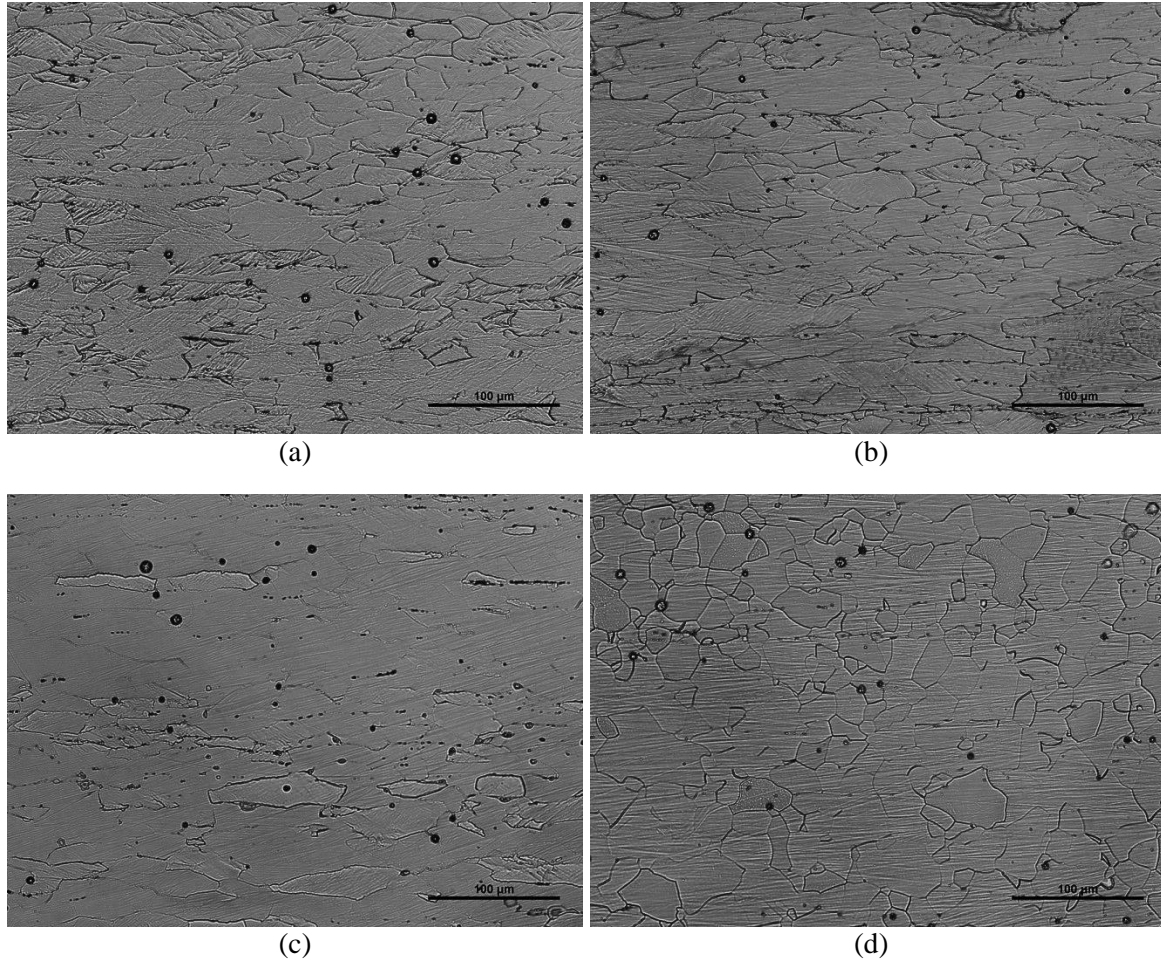
Figure 5. Optical micrographs of the C35M3 samples with the initial thickness reduction of 40%: (a) as-rolled; (b) annealed 4h at 550ºC; (c) annealed 2h at 650ºC; and (d) annealed 1h at 750ºC.

In order to further demonstrate the effect of the selected intermediate annealing (650ºC-1h) on the fabricability of C35M3, stepwise warm-rolling at 300ºC was conducted to simulate a tube fabrication process. The warm-rolling schedule is illustrated in Figure 6. The starting plate (A0) had a thickness of ~2.5mm. The strain per step was ~11% to 26%, reaching a total strain of ~60% in step B4. The intermediate annealing (650ºC-1h) was performed after each rolling step. Sub-sized-dog-bone tensile specimens with gage section dimensions of ~0.5 × 2 × 10 mm were machined by using electrical discharge machining (EDM) from as-rolled and annealed C35M3 with the tensile axis parallel to the rolling direction.
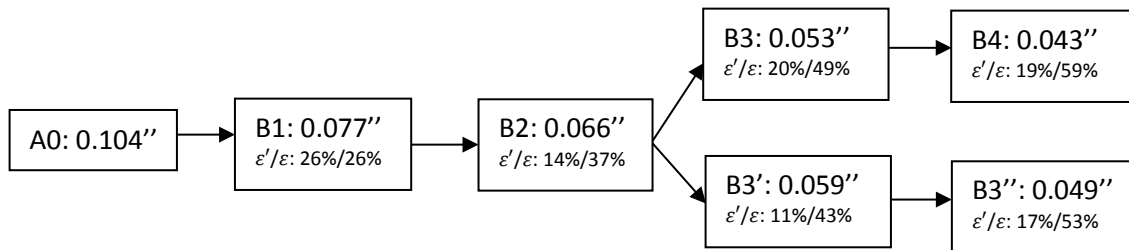
Figure 6. Warm-rolling schedule of C35M3 at 300ºC (ε': strain per step; ε: total strain).

Figure 7 shows the engineering stress vs. engineering plastic strain curves of as-rolled and annealed C35M3 samples, tested at room temperature. The plastic strain was obtained by subtracting the elastic strain from the engineering strain. Note that a suffix character 'a' in the sample ID was used to indicate annealed samples (e.g., B1a). The starting C35M3 plate (A0) had a uniform strain of ~13% with a yield stress of ~490 MPa. However, after warm-rolling, the as-rolled C35M3 specimens exhibited increased yield stress (> ~800 MPa) while the stress immediately dropped after yielding, indicating almost no uniform deformation, as shown in Figure 7a. However, after utilizing intermediate annealing (Figure 7b), the yield stress decreased to a range of ~ 576-680 MPa with improved uniform elongation in the range of 7~8.5%. Figure 8 summarizes the annealing effects on the tensile properties and Vickers hardnesses of the as-rolled and annealed C35M3. A clear relationship is shown between the tensile properties and the hardnesses, indicating that the hardness measurements can be used to determine fabricability after annealing. Optical micrographs of A0, B1, and B3a are displayed in Figure 9 - clearly showing that the grains gradually elongated along the rolling direction from A0 to B3a and no grain growth or recrystallization occurred in B3a.

(a)   (b)
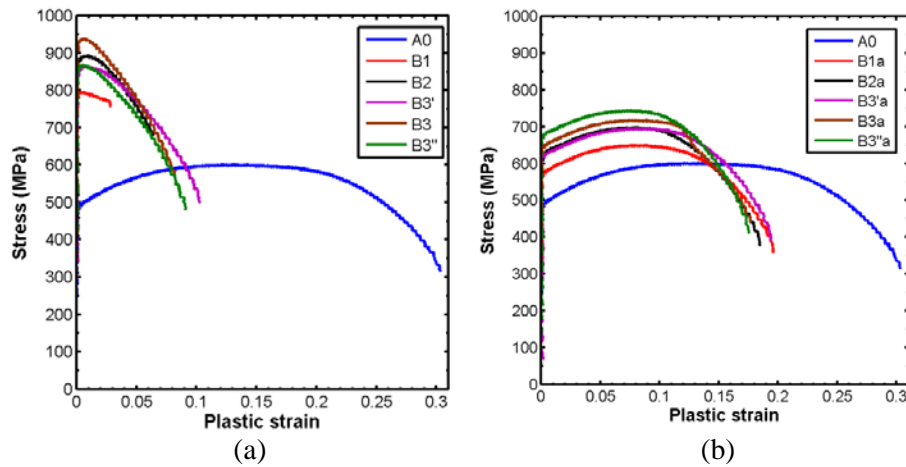
Figure 7. Stress vs. strain curves of C35M3 for (a) as-rolled and (b) annealed samples. The corresponding curve of initial C35M3 plate (A0) is included for comparison.

(a)   (b)   (c)
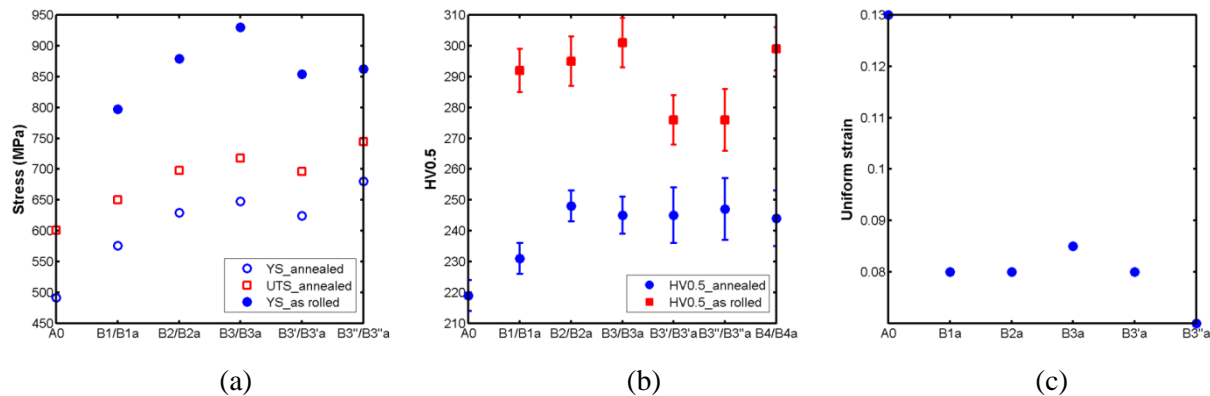
Figure 8. Effects of annealing (650ºC-1h) on (a) tensile properties, (b)Vickers hardness, and (c) plastic uniform strain for rolled C35M3.

(a)	(b)	(c)
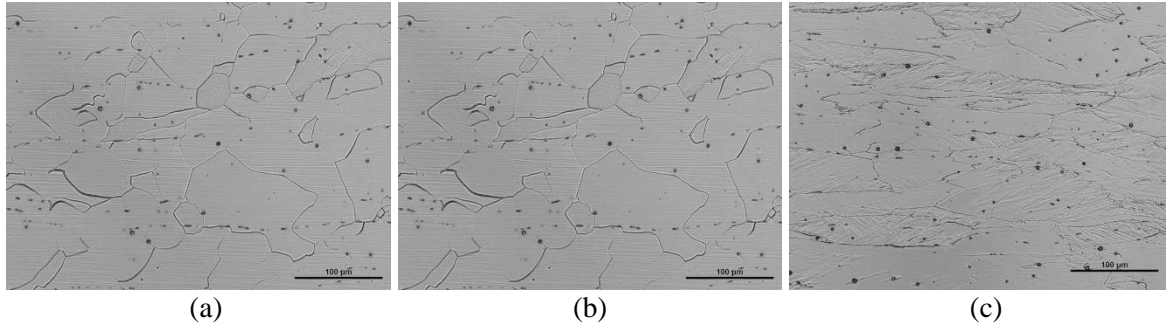
Figure 9. Optical micrographs of the stepwise rolled and annealed C35M3; (a) A0, (b) B1, and (c) B3a.

3.2 Microstructure Evolution during Stepwise Rolling of C35M4 (Simulating Tube-Drawing Process)

Stepwise warm-rolling at 400ºC with intermediate annealing (650ºC-1h or 871ºC-30min) was conducted to simulate tube fabrication of C35M4 (Gen II, Fe-13Cr-5.2Al-2Mo base). The microstructure evolution and mechanical properties during the stepwise rolling were evaluated. The important findings are summarized below:

1) With intermediate annealing at 650ºC for 1 h, C35M4 maintained deformed, non-recrystallized microstructures with grains elongated in the rolling direction. The typical BCC texture consisting of γ-fibre (major) and α-fibre (minor) were developed. The residual strain gradually accumulated as the stepwise rolling proceeded.
2) With intermediate annealing at 871ºC for 30 min, C35M4 exhibited recrystallization and grain growth during the stepwise rolling, resulting in a coarse grain structure with an average equivalent diameter of ~ 200µm. This is not suitable for thin-wall tube production since such coarse grains would cause non-uniform deformation, leading to non-uniform wall thickness.
3) The results demonstrated the coarse grain formation observed at the first trial tube fabrication of C35M2 in FY2015 [12].
4) The intermediate annealing at 650ºC for 1h is considered an optimum intermediate anneal for tube fabrication of C35M4.

Two plates were stepwise warm-rolled at 400ºC with different intermediate annealing steps after each rolling step: (A) 1h at 650ºC and (B) 30min at 871ºC. A total of 16 rolling passes were applied with a nominal 10% thickness reduction per pass. Small coupons for microstructural characterization and hardness measurements were sectioned by EDM after each pass. The measured strain per pass and total accumulated strain are plotted in Figure 10. The measured strain per pass (6.5% - 10.3%) resulted in a final plate thickness of 0.85 mm (total strain ~76.8%) after the 16th pass. In the following section, the as-rolled (annealed) samples after the nth pass are referred as An (An') or Bn (Bn').

11
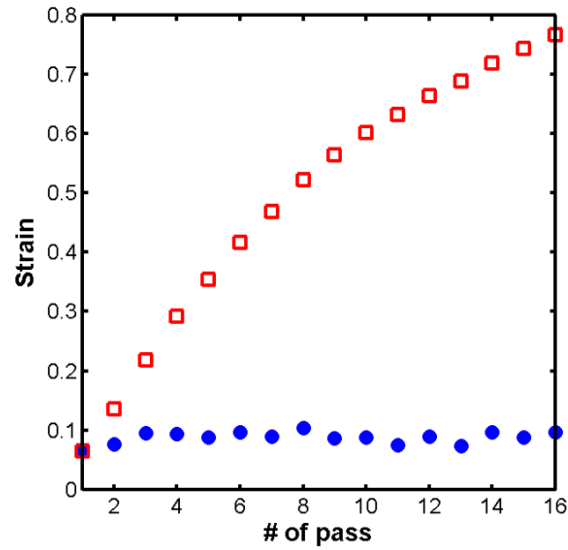
Figure 10. Strain per pass (blue) and total strain (red) in the stepwise warm rolling at 400ºC of C35M4.

3.2.1   Initial state prior to stepwise rolling

A hot-extruded and annealed C35M4 bar sample with an equiaxed grain structure (grain size of ~100um) was prepared. The bar sample was identical to the material that was provided to Rhenium Alloys, Inc. for tube production. Plate samples were sectioned from the extruded bar as starting material for the study. The Vickers hardness prior to stepwise rolling (A0) was 207 ± 6. Figure 11 displays the tensile properties of A0 at 24-800ºC. The yield stress of C35M4 decreased from 490 MPa at room temperature to 89 MPa at 800ºC. The ultimate tensile stress followed a similar trend as a function of temperature. The C35M4 showed considerable deformability with a uniform strain larger than 10% below 600ºC. The uniform strain decreased with temperature above 400ºC, exhibiting ~2% uniform strain at 800ºC, indicating potential deformation instability at elevated temperatures. However, the failure strain increased as the test temperature increased.

(a)   (b)
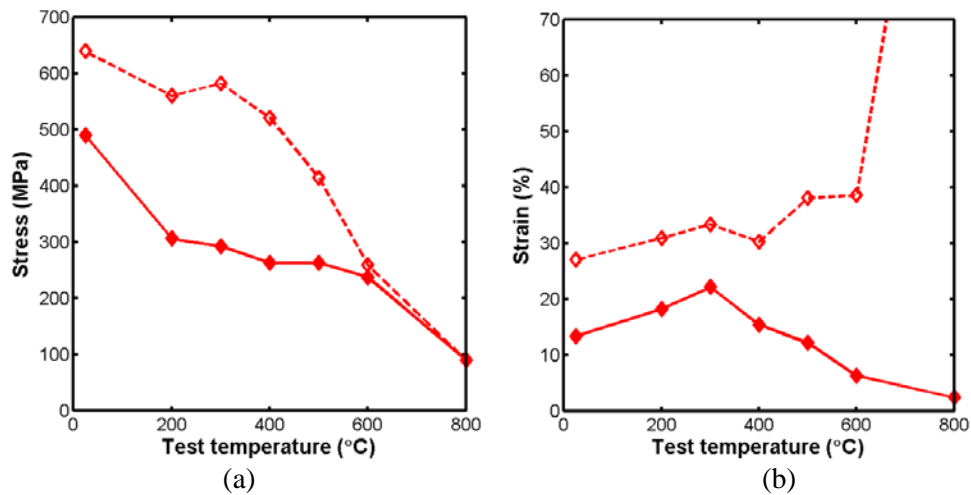
Figure 11. Tensile properties of A0 in a temperature range of 24-800ºC: (a) yield stress (filled symbols)/ultimate tensile stress (open symbols) and (b) uniform strain (filled symbols) and failure strain (open symbols).

3.2.2 Microstructures with the intermediate annealing at 650ºC

Figure 12 shows the inverse pole figure (IPF) maps and (001), (110), and (111) pole figures of A1', A7', and A16', obtained from SEM-EBSD analysis. Note: the rolling direction is parallel to the vertical axis of the IPM maps. As shown in the IPF maps, grains gradually elongated in the rolling direction as the stepwise rolling proceeded. The equivalent average grain diameter slightly decreased from $74 \pm 28 \mu m$ (A1') to $59 \pm 33 \mu m$ (A16'), while the grain aspect ratio significantly decreased from 0.57 ± 0.11 (A1') to 0.12 ± 0.09 (A16'). It is interesting to note that the grain aspect ratio reduction from A1' to A16' was ~ 0.79, which was close to the total thickness reduction. Based on the (001), (110), and (111) pole figures, certain textures were developed in the stepwise rolling. The texture consisting of γ-fibre ({111}<110>, major) and α-fibre ({001}<110>, minor), common in rolled bcc materials, were observed. Subgrains with a size on the order of 1µm were observed in A16', as shown in Figure 13.

Figure 12. Inverse Pole Figure maps and (001), (110), and (111) pole figures of A1' (a & d), A7' (b & e), and A16' (c & f). The EBSD step sizes were 1.0, 0.8, and 0.8µm for A1', A7', and A16', respectively. Note that (a), (b), and (c) have the same size scale.

13
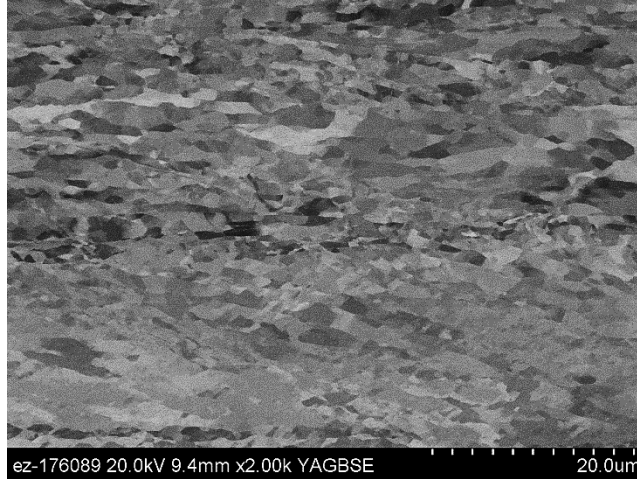
Figure 13. Backscattered electron image of subgrains in A16'.

3.2.3   Microstructures with the intermediate annealing at 871ºC

The IPF maps and (001), (110), and (111) pole figures of B1', B7', and B16' are displayed in Figure 14. In the IPF maps, instead of having deformed and elongated grains, coarse grains were observed in B7' and B16', similar to the results of the first tube fabrication trial in FY2015 [12]. The average equivalent grain diameter increased from $73 \pm 29\mu m$ (B1') to $172 \pm 59\mu m$ (B16'). The grain aspect ratio slightly dropped from 0.57 ± 0.10 (B1') to 0.42 ± 0.09 (B7'). However, it went back to 0.49 ± 0.15 in B16'. No clear texture tendency was observed in B7' and 16', as demonstrated in the pole figures.

3.2.4   Mechanical properties after the stepwise rolling

The Vickers hardness of as-rolled and annealed C35M4 after the 1st, 4th. 7th, and 16th passes are plotted in Figure 15. The Vickers hardness after the 1st rolling pass increased from 207 ± 6 (A0) to ~250 (A1 and B1). Note that the hardness of the as-rolled samples was always higher than the starting material and the highest hardness reached was ~280. The intermediate annealing always lowered the hardness of the rolled C35M4 samples, as shown with the open symbols in Figure 15. With the intermediate annealing at 650ºC, the hardness of the annealed C35M4 samples increased initially and saturated at ~240, indicating that the accumulated residual strain balanced with the recovering process (without recrystallization). The hardness of the annealed samples maintained an almost constant value of ~210 with the intermediate anneal at 871ºC. Based on the microstructural characterization and Vickers hardnesses, it is concluded that the intermediate anneal of 871ºC, 30 min is not suitable for tube drawing of C35M4 because it would not prevent recrystallization and grain growth.
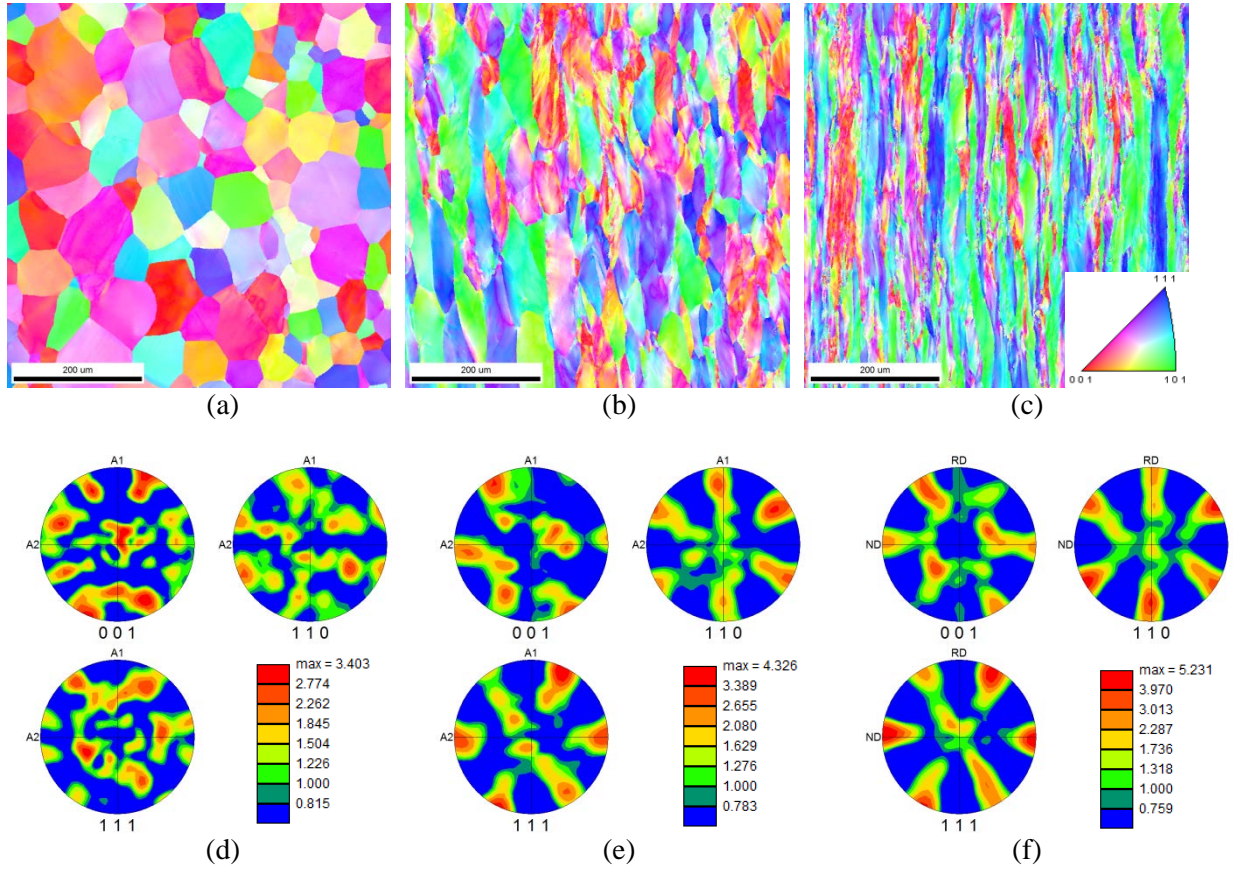
14

(a)   (b)   (c)

(d)   (e)   (f)

Figure 14. IPF maps and (001), (110), and (111) pole figures of B1' (a & d), B7' (b & e), and B16' (c & f). The EBSD step sizes were 1.0, 0.8, and 0.8µm for A1', A7', and A16', respectively. Note that (a), (b), and (c) have the same size scale.
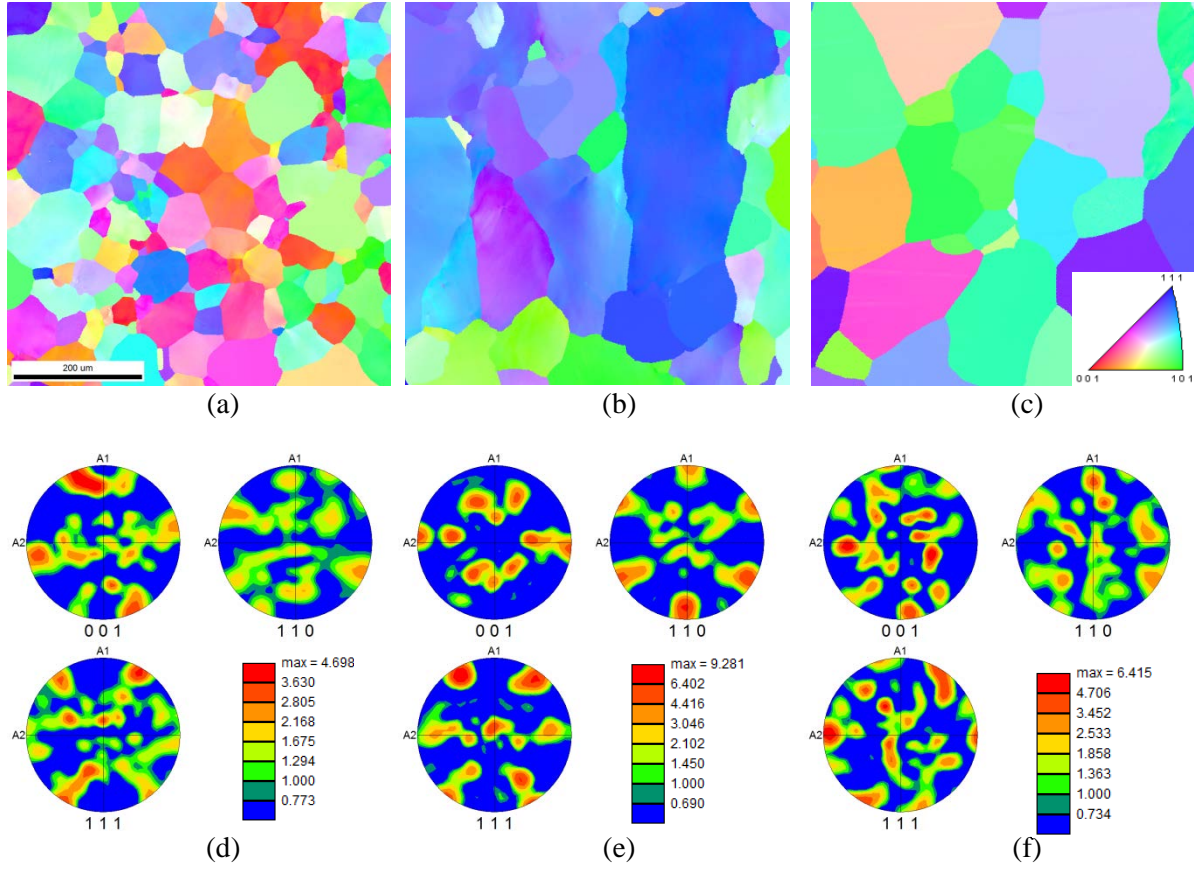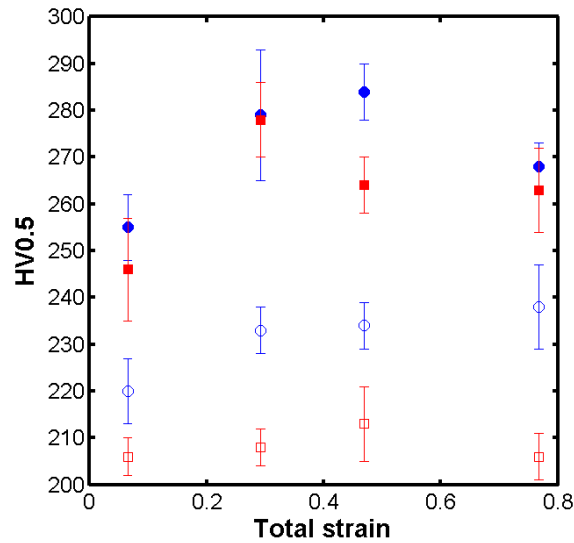

Figure 15. Vickers hardness of as-rolled (filled markers) and annealed (unfilled markers) C35M4 samples after the 1st, 4th, 7th, and 16th passes (blue: 650ºC-1h; red: 871ºC-30min).

3.3 Microstructural Control of Nb-containing FeCrAl Alloys

The addition of Nb to FeCrAl alloys is known to promote the formation of sub-micron size Fe_2Nb-Laves phase particles during warm- or hot-processing which effectively stabilize the deformed microstructure and improve mechanical properties at both room and elevated temperatures [11,12]. In order to utilize the beneficial effect of such Laves-phase formation, it is important to understand the relationship among the alloy composition, microstructure, deformability, and the stability of the deformed microstructure. In this section, the recovery and recrystallization behaviors of several Nb-containing FeCrAl alloys at 600-900ºC were investigated in order to understand the effects of Nb on the microstructural stability and mechanical properties of FeCrAl alloys. Based on the results, it is concluded that; (1) the recovery and recrystallization kinetics of the warm-rolled materials is not sensitive to the Cr content in a range from 11 to 13 wt.%; and (2) the thermal stability of deformed microstructures increases with increased Nb content up to 1 wt.%, whereas the stability becomes less dependent on the Nb content with additions greater than 1 wt.%. Optimization of the process conditions for tube-production is still required because the higher strength, compared to Mo-containing FeCrAl alloy, needs to be balanced with tube fabricability. The optimization effort is in progress.

Five different Nb-containing FeCrAl alloys (C16N, C26N, C36N, C36N2, and C36N3, Fe-{11-13}Cr-6Al-{0.7-2}Nb base) were investigated. Some results of C36M2 (Fe-13Cr-6Al-2Mo base) were included for comparison. All alloys were hot-rolled and annealed at 1200°C to prepare the starting plate materials with 2.5mm thickness and a grain size of ~100µm. The starting plates were warm-rolled at 300°C with 10% thickness reductions per pass, total ~ 80% thickness reductions. Warm-rolled plates were sectioned into small pieces and then annealed at 600-900ºC for durations up to 504h.

3.3.1 Microstructures of deformed samples

As shown in Figure 16a, as-rolled samples exhibited a band-like microstructure consisting of grains elongated in the direction of rolling. The IPF map of the as-rolled C36N in Figure 16b showed a variation of misorientation in each elongated grain, indicating deformation inhomogeneity within and among grains. A few Laves phase particles with a volume fraction of $1.6 \pm 0.2\%$ and an equivalent radius of $\sim 1.2 \pm 0.4$ µm were observed in the as-rolled C36N2. Only small amounts of Laves phase particles were observed in the as-rolled C36N, indicating that the Nb solution limit in bcc-Fe matrix at 1200°C was close to 1 wt.% in the current FeCrAl alloys. Cracks were occasionally observed in the Laves phase particles (Figure 16c), but they did not propagate into the bcc-Fe matrix, suggesting that the brittleness of the particles would not degrade the deformability of the alloys. The as-rolled Vickers hardnesses were 378 ± 8 (C16N), 386 ± 7 (C26N), 394 ± 6 (C36N), 423 ± 8 (C36N2), 382 ± 11 (C36N3), and 359 ± 12 (C36M2).

16

(a)   (b)

(c)
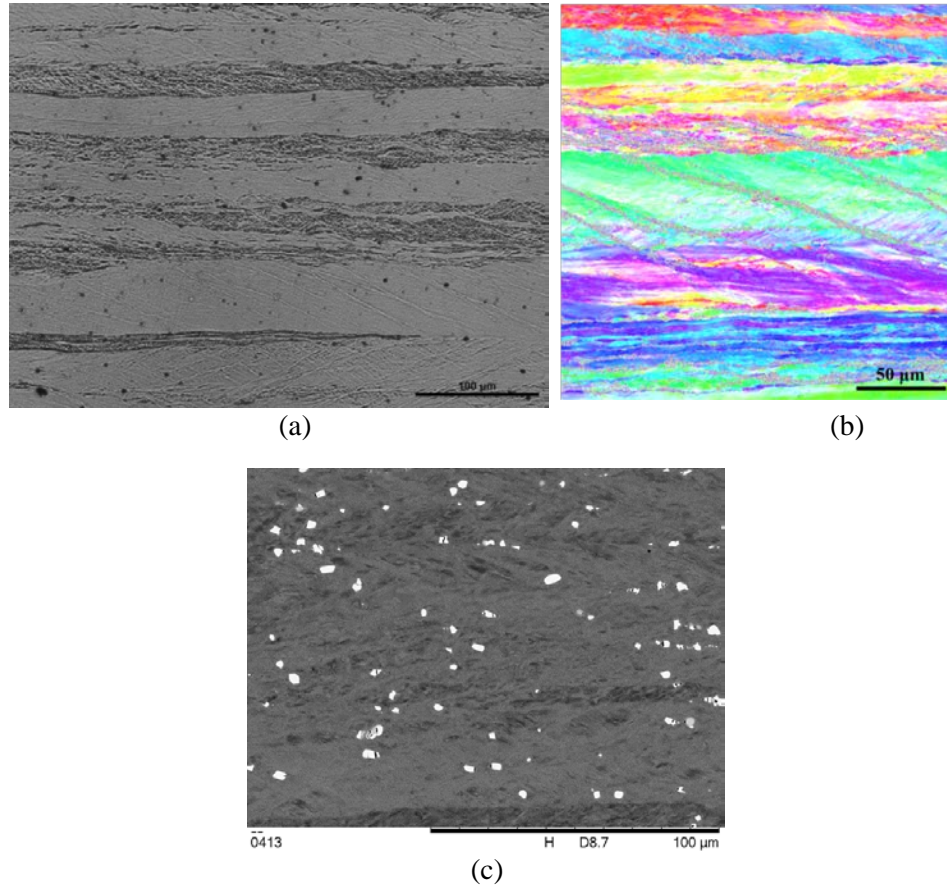
Figure 16. (a) Typical optical micrographs of as-rolled specimens showing band-like structures along the rolling direction; (b) IPF map of the as-rolled C36N sample; and (c) back-scattered electron image of the as-rolled C36N2 sample showing Laves phase particles (with bright contrast).

3.3.2   Microstructures of annealed samples

Recovery and recrystallization occurred during annealing. Figure 17 shows the recrystallization initiation time of the studied alloys at 650-800℃ (observed under optical microscopy). C16N, C26N, C36N, and C36N2 had similar recrystallization kinetics, and thus, only the results of C36N were displayed in Figure 17. By comparing the recrystallization initiation time of C36M2 (0Nb), C36N3 (0.7Nb), and C36N (1 or 2Nb), it is clear that the Nb addition in FeCrAl alloys significantly stabilizes the deformed microstructures up to 1 wt.%, and no further stabilization is expected with more than 1 wt.% addition.

17
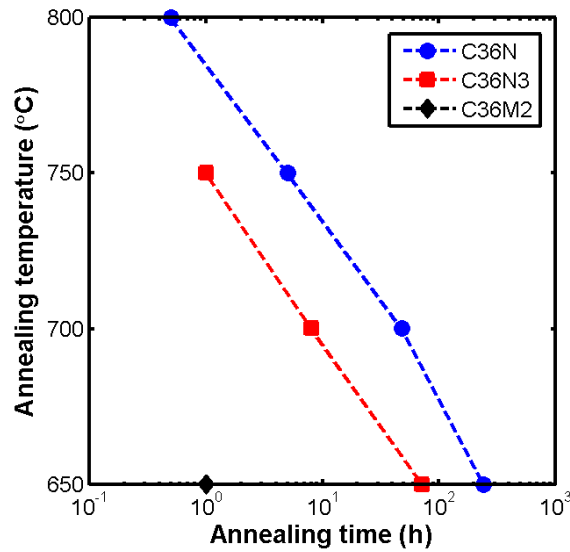
Figure 17. Initiation of recrystallization at 650-800ºC observed by optical microscopy for C36N (1Nb), C36N3 (0.7Nb), and C36M2 (0Nb).

Microstructural details and mechanical properties after annealing will be discussed next. The IPF map of C36N after annealing for 1h at 700ºC is displayed in Figure 18a. Note that the rolling direction is parallel to the horizontal axis of the IPF maps. Some areas had larger rotations compared to the surroundings, which were likely heavily deformed during warm-rolling. These areas were found to have equiaxed subgrains, ~1µm in size, with high-angle boundaries upon further annealing at 700ºC, as shown in Figure 18b. Moreover, elongated recrystallized grains (~10µm in size) formed by consuming the fine grains. Several grains having low internal misorientation did not show clear sub-boundaries in the IPF map (Figure 18b). SEM back-scattered electron images of the annealed C36N indicated that the Laves phase particles (bright contrast) pinned grain/subgrain boundaries, as shown in Figure 18c and Figure 18d. It is interesting to note that two distinct microstructures were observed in Figure 18c; one with mostly equiaxed subgrains (~1µm in size) with less and larger Laves phase particles, and the others with fine elongated subgrains with smaller Laves phase particles.

Recrystallization initiated quickly when annealed at higher temperatures (e.g., 800 and 900ºC). Figure 19a shows the mixed microstructures of C36N annealed for 24h at 800ºC. Reaction fronts (high-angle grain boundaries) advancing into non-recrystallized region were observed (marked by arrows in Figure 19). C36N had smaller recrystallized grains at 900ºC than those at 800ºC as can be seen by comparing Figure 19a and Figure 19b. Figure 19b also shows recrystallized grains (~23.5 $\pm$ 14.4µm in equivalent diameter) elongated in the rolling direction with a grain aspect ratio of 0.3 $\pm$ 0.1. There were still a few non-recrystallized grains (marked by arrows in Figure 19b) with subgrains in C36N annealed for 24h at 900ºC. The (001), (110), and (111) pole figures of Figure 19b are displayed in Figure 19c. Based on these pole figures, no strong texture was observed in recrystallized grains of C36N after annealing for 24h at 900ºC. Back-scattered electron images of C36N samples annealed at 900ºC for 1h and 72h are shown in Figure 20a and Figure 20b, respectively. In Figure 20a, a large number of Laves phase particles remained within recrystallized grains. However, after annealing for 72h at 900ºC, most of Laves phase particles were distributed along grain boundaries with few Laves phase particles within recrystallized grains.

18

(a)   (b)

(c)   (d)
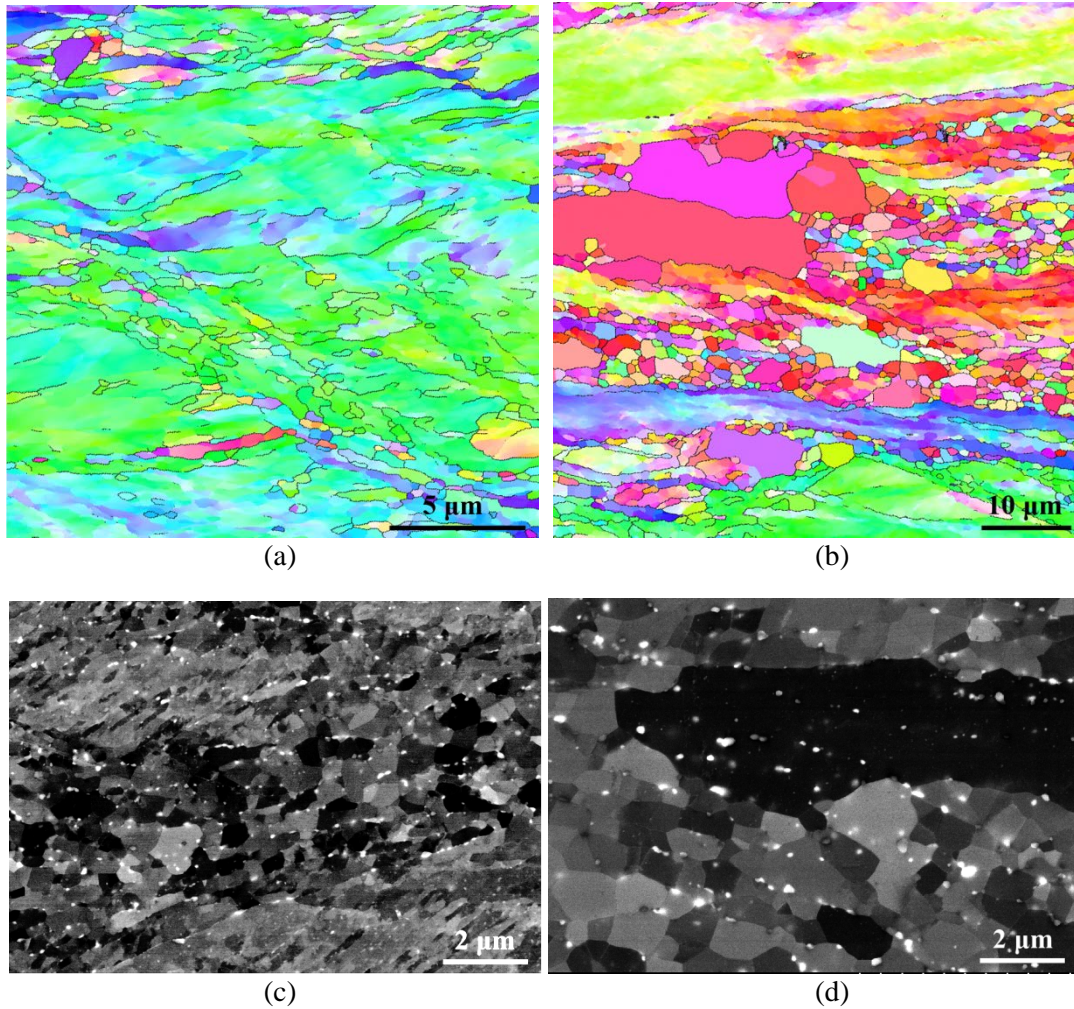
Figure 18. IPF maps of C36N samples after annealing at 700°C for (a) 1h and (b) 96h. Grain boundaries with misorientation greater than 15° would be marked by black lines. Backscattered electron images shows Laves phase particles (bright contrast) and subgrains in C36N samples annealed at 700°C for (c) 8h and (d) 96h.
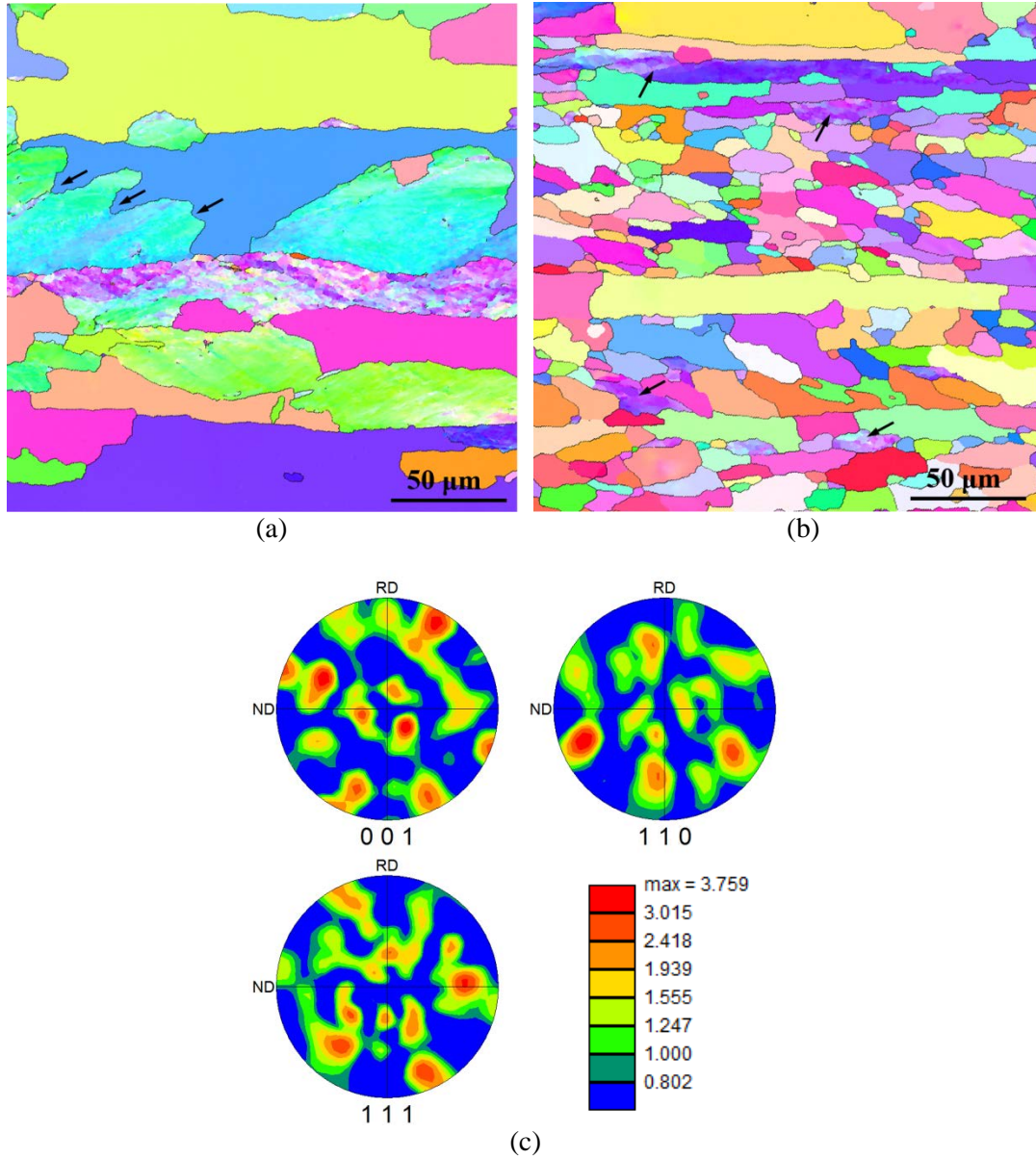
Figure 19. IPF maps of C36N samples after annealed for 24h at (a) 800ºC and (b) 900ºC. Grain boundaries with the misorientation greater than 15° are marked by black lines. The (001), (110), and (111) pole figures of (b) are shown in (c).
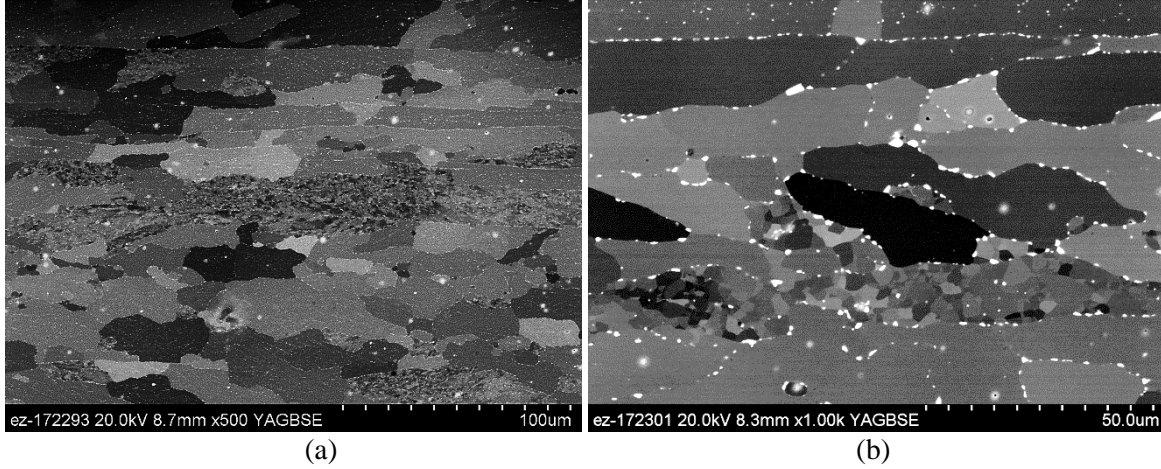
Figure 20. Backscattered electron images of C36N samples annealed at 900ºC for (a) 1h and (b) 24h.

3.3.3   Mechanical properties of deformed and annealed samples

Figure 21a shows the annealing effects on the Vickers hardness of C36N at 600-900ºC. Overall, the hardness decreased as the annealing time increased. There were hardness plateaus at 600, 650, and 700ºC, where the hardness slightly decreased or stayed constant. All other Nb-containing FeCrAl alloys showed similar trends with C36N. Figure 21b compares the annealing effects on C36N, C36N2, C36N3, and C36M2 at 700ºC. As shown in Figure 21c, the annealing treatment softened as-rolled C36N and increased its deformability.
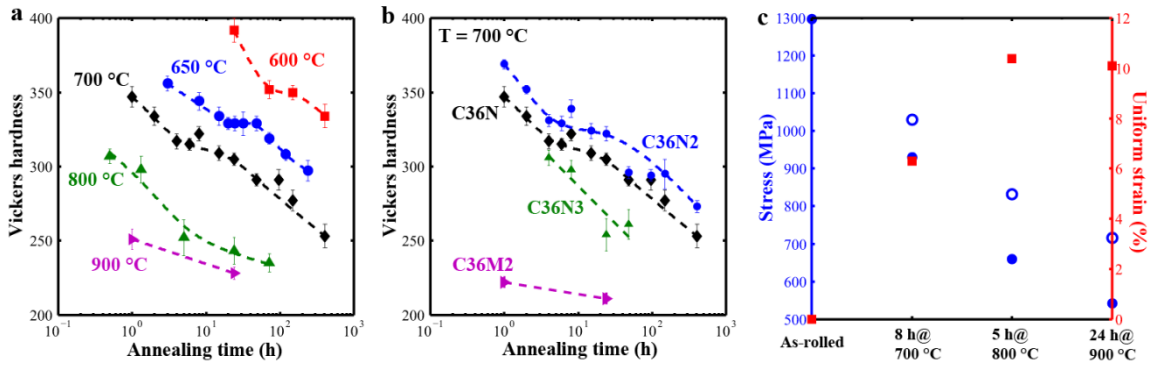
Figure 21. (a) Effect of annealing at 600-900 ºC on the Vickers hardness of C36N samples; (b) Comparison of the annealing effect at 700 ºC on the Vickers hardness of C36N, C36N2, C36N3, and C36M2 samples; (c) Tensile properties of as-rolled and annealed C36N samples.

21

4. ATF FECRAL TUBE PRODUCTION VIA COMMERCIAL MANUFACTURERS

4.1 Tube Drawing at Century Tubes, Inc.

Century Tubes, Inc. (CTI) successfully produced thin-wall FeCrAl alloy tubes of both Gen I and Gen II alloys through cold-drawing and annealing. It was found that the control of grain structure (preventing grain coarsening) would be the key to better tube fabricability, uniform wall thickness, and (potentially) improved mechanical properties of final tube products. CTI produced thin-wall tube products of Gen I B126Y (total ~21ft length) and Gen II C06M2 (total ~5ft length) alloys in FY2016. Additional tube production of Gen II C36M3 (expected 10ft length) and Gen I B136Y3 (expected 250ft length) is currently in progress, and the expected delivery date is in the middle of June and the end of July, respectively.

In FY2014, CTI successfully produced thin-wall seamless tubes of the Gen I model FeCrAl alloys, Fe-13Cr-4.5Al-Y (T35Y2) and Fe-15Cr-4Al-Y (T54Ys) [11]. CTI used tube-drawing processes at room temperature, combined with intermediate annealing. The detailed process parameters were proprietary. Although the first thin-wall tube production was successful, the microstructure consisted of coarse grains (~100-200µm in size) which were not suitable in terms of mechanical properties. Tube-burst testing of the sealed tubes was carried out at ORNL. They exhibited relatively poor barreling deformation resistance - bursting during the ramp test [12]. Microstructural characterization clearly showed some of the coarse grains with heavily deformed features, resulting in strain concentration which leads to premature failure. This suggests that microstructural control, especially for grain refinement, would play an important role in the properties of tube products.

CTI also produced thin-wall FeCrAl alloy tubes of Gen II modified FeCrAl alloys, Fe-10Cr-6Al-2Mo base (C06M2), as shown in Figure 22. Optimized process parameters for C06M2 successfully controlled the microstructure with fine and uniform grains (~10-20µm in size). The small grain size was beneficial (and required) for obtaining uniform wall thickness of the tube product. The detailed cross-sectional characterization results are shown in Figure 23, which clearly indicated better concentricity compared to C35M3 tube produced by RAI in FY2015 [12].

Based on these results, close attention will be required during current tube production at CTI to prevent unnecessary grain coarsening during the tube fabrication processes as well as in the final tube products. The recently-procured tubes (C36M3 and B136Y2) will be characterized in a similar way and evaluated for property screening including tensile testing, oxidation testing, and irradiation testing.

4.2 Tube Drawing at Rhenium Alloys, Inc.

Rhenium Alloys, Inc, (RAI) has been working with ORNL on FeCrAl tube fabrication using the warm-drawing process. Several trials to process or produce the Gen II FeCrAl alloy tubes, such as C35MN5B (Fe-13Cr-5.2Al-2Mo-1Nb-0.2Si-Y), C35M3 (Fe-13Cr-5.2Al-2Mo-0.2Si-Y), C36M2 (Fe-13Cr-6Al-2Mo-0.2Si-Y), and C37M (Fe-13Cr-7Al-2Mo-0.2Si-Y), were conducted. Only C35M3 was successfully tube-drawn to achieve the target outer diameter, but the final wall thickness was not uniform. This was due to unexpected grain coarsening during non-optimized intermediate annealing, as summarized in the previous report [12] or Section 3.2.3. The other tube drawings of C35MN5B, C36M2, and C37M resulted in premature failure early in the warm-drawing [12] reduction process. These failures did provide important data points regarding FeCrAl deformability; specifically on the effect of alloying additions on work hardening, initial microstructure, hardness control prior to the tube drawing, the upper limit of the area reduction without intermediate annealing, the effect of intermediate annealing conditions, and so on.
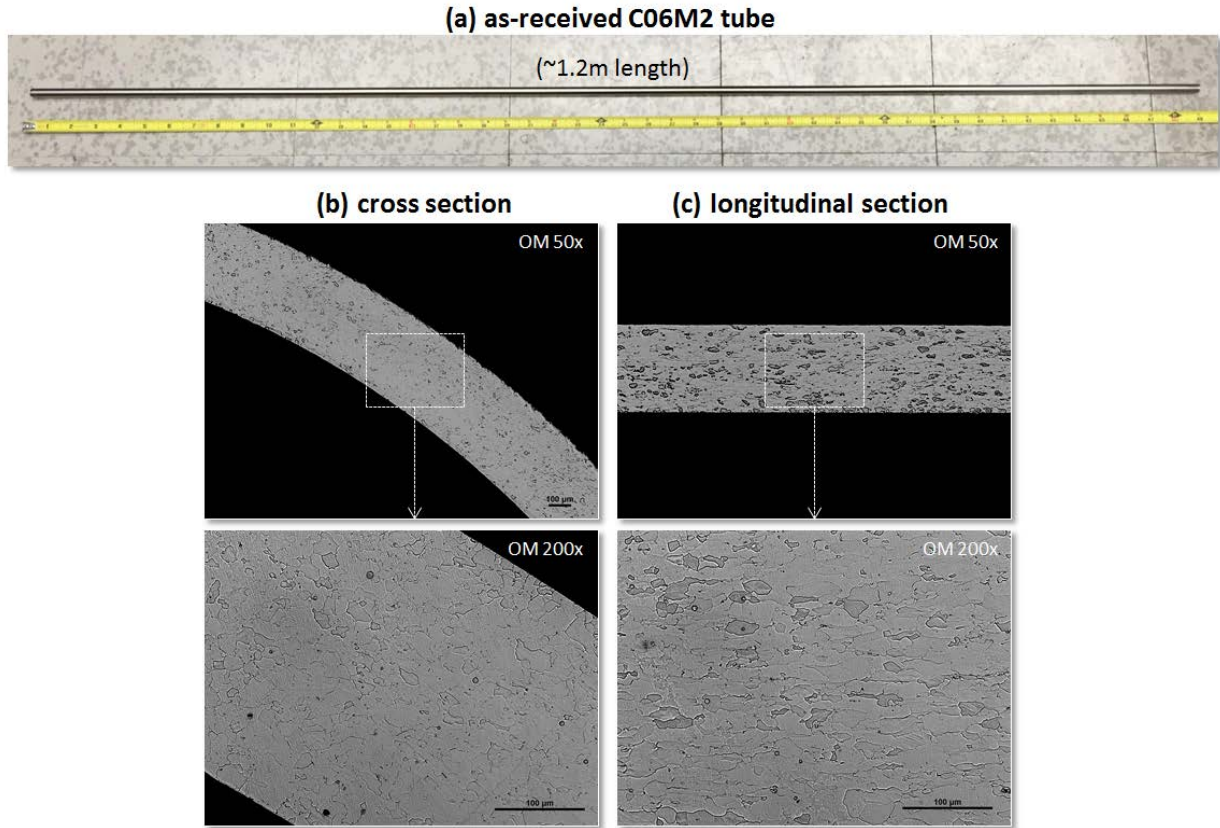
Figure 22. As-received C06M2 thin wall tube produced by CTI; a picture of whole tube (a), and optical micrographs of cross section (b) and longitudinal section (c).

Table. Wall thickness (t, μm) of C06M2 tube.

	A	B	C	D	E	F	G	H
t	390	394	391	384	380	366	369	375

$\bar{t}$ = 381 $\pm$ 10, E = 7%

Figure 23. Optical micrograph montage of cross-sectional view of as-received C06M2 tube, together with a list of wall thickness at various locations.

The large-quantity tube production of C35M4 alloy is currently in progress at RAI with the aim to produce a total of 250ft length in tubes. The suggested process parameters based on the effort in sections 3.1 and 3.2 has been shared with RAI, and is utilized in the current process. RAI has been performing microstructural characterizations and the hardness analyses at each process step (after drawing and annealing) to monitor that there are no strange microstructural features or hardness changes during this process. The expected completion date is in the middle of June. Once the production is completed, the recently-procured tubes (C35M4) are to be characterized in similar way to the previous tubes, and evaluated for property screening including tensile testing, oxidation testing, and irradiation testing.
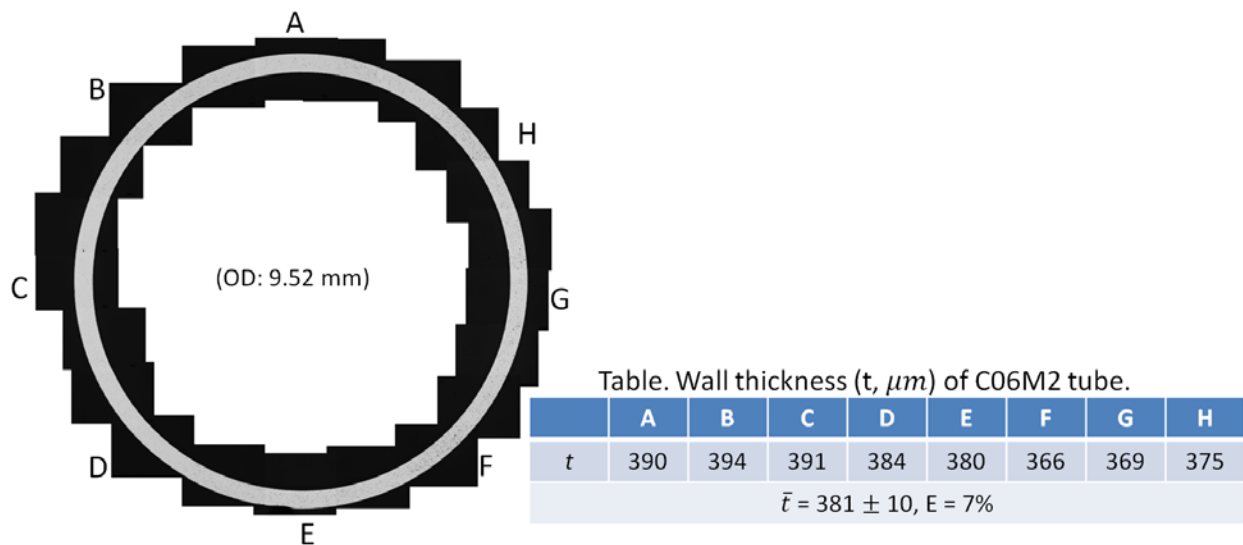
4.3   Pilgering at Superior Tube Company, Inc.

The cold-pilgering process is one of the major industrial tube fabrication processes. It is suitable for continuous tube mass production. It is not easily adaptable for lab-scale tube production evaluation using the existing equipment at commercial manufacturers as it requires stopping the current production process. However, it is a very attractive process for FeCrAl tube production since the deformation sequence during reduction is almost identical to the conventional rolling process, indicating that much less force is required during processing (i.e. eliminating the frictional forces inherent in the tube-drawing process). In addition, the pilgering process is basically a compressive process such that the materials are less likely to tear compared to the tensile processes in tube-drawing. Therefore, it is worthwhile to attempt the tube production through the pilgering process to evaluate how the process would be beneficial for FeCrAl tube production (e.g. widen the process window to make potential mass tube production easier in the future).

Superior Tube Company, Inc. (STC) has agreed to support the lab-scale tube production of FeCrAl alloys. The extruded and annealed bars of C06M2 and C36M3 alloys were provided. These were identical to the materials processed/being processed at CTI. Therefore, direct comparison of tube production between the drawing and the pilgering processes is expected. The bar materials were gun-drilled at the end of May. The detailed discussion of process parameters has been initiated between STC and ORNL. The delivery date has not been scheduled yet, but is expected in July/August in 2016.

5.   SUMMARY

Two major concerns in ATF FeCrAl alloy tube production have been discussed in this report; (1) optimization of microstructural control of ATF FeCrAl alloys during the tube drawing process, and (2) provision of an update on the progress of ATF FeCrAl tube production via commercial manufacturers.

Experimental efforts have been made to optimize the process parameters balancing tube fabricability, especially for tube drawing processes, and microstructure control of the final tube products. Lab-scale sheet materials of Gen II FeCrAl alloys (Mo-containing and Nb-containing FeCrAl alloys) were used in the study, combined with a stepwise warm-rolling process and intermediate annealing, simulating the tube drawing process at a commercial tube manufacturer. The intermediate annealing at 650ºC for 1h was recommended for tube-drawing processes of Mo-containing FeCrAl alloys (C35M4, Fe-13Cr-5.2Al-2Mo base) because it successfully softened by recovering the work hardening introduced through the rolling step, without any grain coarsening occurring from recrystallization. The final tube product is expected to have a stabilized deformed microstructure providing improved tensile properties with sufficient ductility. In contrast, the intermediate annealing at 871ºC for 30min resulted in grain coarsening due to recrystallization during processing, leading to potentially non-uniform wall thickness observed in C35M2 in FY2015 [12]. Optimization efforts on Nb-containing FeCrAl alloys focused on the effect of alloying additions and annealing conditions on the stability of the deformed microstructure. Relationships between the second-phase precipitates (Fe_2Nb-Laves phase) and microstructural stability was discussed.

FeCrAl tube production through commercial tube manufacturers is currently in progress. Three different manufacturers, Century Tubes, Inc. (CTI), Rhenium Alloys, Inc. (RAI), and Superior Tube Company, Inc. (STC) are involved, each having a capability of cold-drawing, warm-drawing, and HPTR cold-pilgering, respectively. CTI successfully manufactured two FeCrAl alloy tubes, Gen II C06M2 (Fe-10Cr-6Al-2Mo base) and Gen I B126Y (Fe-12Cr-6Al base) alloys. Microstructural characterization revealed that C06M2 consisting of a refined grain structure with 10-20µm grain size, contributed to the successful production of a thin-wall tube with uniform wall thickness. CTI and RAI are currently working on the large-quantity tube production (expected 250ft length) of Gen I model FeCrAl alloy (B136Y3, at CTI) and Gen II (C35M4, at RAI), with the process parameters obtained from the experimental efforts. The expected delivery dates are the end of July, 2016, and the middle of June, 2016, respectively. For STC, this will be the first attempt to apply cold-pilgering to the FeCrAl alloys. Communication has been initiated and the materials have been machined for the cold-pilgering process.

6.   REFERENCES

[1]   Powers, D.; Meyer, R. Cladding swelling and rupture models for LOCA analysis, NUREG-0630; U. S. Nuclear Regulatory Commission: 1980.
[2]   B. A. Pint, K. A. Unocic and K. A. Terrani, Materials at High Temperature, 32 (2015) 28-35.
[3]   M. Moalem, D.R. Olander, Journal of Nuclear Materials 182 (1991) 170.
[4]   K. Suzuki, S. Jitsukawa, N. Okubo, F. Takada, J.Nucl.Eng. and Design 240 (2010) 1290–1305.
[5]   M. Steinbrück, M. Große, L. Sepold, J. Stuckert, Nuclear Engineering and Design 240 (7) (2010) 1714-1727.
[6]   Y. Yamamoto, B.A. Pint, K. Terrani, K.G. Field, L.L. Snead, "Letter report documenting identifying billets and alloys fabricated for distribution to program" M3FT-13OR0202291, ORNL/LTR-2013/322, Oak Ridge National Laboratory (2013).

[7]   P. Grobner, Metallurgical and Materials Transactions B, 4 (1973) 251-260.

[8]   K.G. Field, X. Hu, K.C. Littrell, Y. Yamamoto, L.L. Snead, "Radiation Tolerance of Neutron-Irradiated Model Fe-Cr-Al Alloys," Journal of Nuclear Materials, 465 (2015) 746-755.

[9]   K.G. Field, M.N. Gussev, Y. Yamamoto, L.L. Snead, "Deformation behavior of laser welds in high temperature oxidation resistant Fe-Cr-Al alloys for fuel cladding applications," Journal of Nuclear Materials, 454 (2014) 352-358.

[10] B. A. Pint, S. Dryepondt, K. A. Unocic, and D. T. Hoelzer, JOM, 66 (2014) 2458-2466

[11] Y. Yamamoto, Y. Yang, K.G. Field, K. Terrani, B.A. Pint, and L.L. Snead, "Letter Report Documenting Progress of Second Generation ATF FeCrAl Alloy Fabrication, FY14 FCRD milestone report," M3FT-14OR0202232, ORNL/LTR-2014/219, Oak Ridge National Laboratory (2014).

[12] Y. Yamamoto, M.N. Gussev, B.K. Kim, T.S. Byun, "Optimized properties on base metal and thin-walled tube of Generation II ATF FeCrAl", M2FT-15OR0202291, ORNL/TM-2015/414 (2015).

[13] B.A. Pint, K.A. Unocic, K.A. Terrani, "Steam Oxidation of FeCrAl and SiC in the SATS", M3FT-15OR0202342, ORNL/LTR-2015/417 (2015).

[14] K.A. Terrani, S.J. Zinkle, L.L. Snead, "Advanced Oxidation-resistant Iron-based Alloys for LWR Fuel Cladding," Journal of Nuclear Materials, 448 (2014) 420-435.

[15] H. Qu, Y. Lang, C. Yao, H. Chen, C. Yang, Materials Science and Engineering: A 562 (2013) 9-16.

[16] "Shanghai EverSkill M&E Co., Ltd": *http://www.esmeind.com/Pro-Tube.html#*

[17] "Cold Pilger Rolling: Part One" in the website of Total Materia, Apr. 2013: *http://www.totalmateria.com/page.aspx?ID=CheckArticle&site=kts&NM=396*

[18] Albert Nerino, Mark Deaver, Chris Nagele, John Reinhart , "HPTR's past, present, and future — Part I", TPJ - THE TUBE & PIPE JOURNAL® , Jun. 2011: *http://www.thefabricator.com/article/tubepipeproduction/hptras-past-present-and-future-a-part-i*